Hindawi
International Journal of Photoenergy
Volume 2020, Article ID 6150794, 11 pages
https://doi.org/10.1155/2020/6150794

Research Article

Thermomechanical Fatigue Behavior of Spray-Deposited SiC_p/Al-Si Composite Applied in the High-Speed Railway Brake Disc

Wei Li,[1,2] **Huitao Chen**,[1,2] **Lu Zuo**,[1,2] **Jian Chen**,[1,2] **Dongliang Xu**,[1,2] **Jianjun He**,[1,2] **Cong Li**,[1,2] **Zhuoyin Peng**,[1,2] **Yanjie Ren**,[1,2] **and Sheng-de Zhang**[3]

[1]*Key Laboratory of Efficient & Clean Energy Utilization, School of Energy and Power Engineering, Changsha University of Science & Technology, Changsha 410114, China*
[2]*Hunan Province 2011 Collaborative Innovation Center of Clean Energy, and Smart Grid, Changsha 410114, China*
[3]*Japan Electric Power Central Research Institute, Tokyo 240-0196, Japan*

Correspondence should be addressed to Wei Li; lwzzgjajie@126.com and Jian Chen; chenjian_513@126.com

Received 6 November 2019; Accepted 10 January 2020; Published 7 February 2020

Guest Editor: Hafiz M. Ali

The thermomechanical fatigue (TMF) behaviors of spray-deposited SiC_p-reinforced Al-Si alloy were investigated in terms of the size of Si particles and the Si content. Thermomechanical fatigue experiments were conducted in the temperature range of 150-400°C. The cyclic response behavior indicated that the continuous cyclic softening was exhibited for all materials, and the increase in SiC particles size and Si content aggravated the softening degree, which was attributed to dislocation generation due to differential thermal contraction at the Al matrix/Si phase interface or Al matrix/SiC particle interface. Meanwhile, the TMF life and stress amplitude of SiC_p/Al-7Si composites were greater than those of Al-7Si alloy, and increased with the increasing SiC particle size, which was associated with "load sharing" of the direct strengthening mechanism. The stress amplitude of 4.5μmSiC_p/Al-Si composite increased as the Si content increased; however, the influence of Si content on the TMF life was not so significant. The TMF failure mechanism revealed that the crack mainly initiated at the agglomeration of small-particulate SiC and the breakage of large-particulate SiC, and the broken primary Si and the exfoliated eutectic Si accelerated the crack propagation.

1. Introduction

The depletion of natural resources and environmental pollution are major challenges facing humanity today. It is urgent to study new energy sources instead of traditional fossil energy sources. The use of clean energy such as solar energy has been very extensive. For instance, new energy vehicles are using clean energy to save resources and protect the environment [1]. However, the development of new technologies has improved the requirements of materials. For instance, the light-weight, wear resistance, and thermomechanical fatigue properties of composites for automotive brake discs are very important [2–4]. The traditional metal brake discs are easy to crack and cannot ensure the safety of the vehicles due to the high temperature produced by friction between wheel and rail with high driving speed (≥400 km/h). Some new composites like carbon/carbon fiber-reinforced carbon matrix composites have excellent high-temperature wear resistance, but oxidation and high manufacturing cost restrict their widespread application. SiC_p/Al-Si composite, owing to advantages such as high-specific strength, excellent thermal conductivity, and low expansion coefficient, is considered as an ideal metal matrix composite (MMC) for brake disc [5–8]. In the process of actual braking, the residual stress caused by the mismatch in thermal-expansion coefficient (CTE) between SiC particle and Al-Si alloy while the composites are subjected to mechanical load leads to thermomechanical fatigue (TMF) collaboratively.

Several methods can be adopted to prepare the SiC_p/Al-Si composites such as stir casting [9], powder metallurgy [10], and spray deposition [11]. Spray deposition is a rapid prototyping process to gas atomize a stream of molten metal by mean of high velocity gases (i.e., Ar or N_2) and to direct the resulting spray into a cold substrate [12]. Not only can this

Table 1: Composition of materials.

Materials	SiC particle size (μm)	Si (wt%)	Mg (wt%)	Mn (wt%)	Cu (wt%)	Al (wt%)
Al-7Si	0	7	0.3	0.01	0.01	Bal.
20μmSiC_p/Al-7Si	20	7	0.3	0.01	0.01	Bal.
4.5μmSiC_p/Al-7Si	4.5	7	0.3	0.01	0.01	Bal.
4.5μmSiC_p/Al-13Si SiC_p/Al-13Si	4.5	13	0.3	0.01	0.01	Bal.
4.5μmSiC_p/Al-20Si	4.5	20	0.3	0.01	0.01	Bal.

method avoid the oxidation reaction between molten metal and bubbles during stirring process [13] but also make some microstructure improvements such as refining the grains, decreasing the segregated phase, and making the internal SiC particles more evenly distributed in SiC_p/Al-Si composite [14]. Generally, the material prepared by spray deposition has high strength, good plasticity, and strong wear resistance [15].

There are many factors affecting the TMF properties of MMCs, involving complex mechanism. The in-phase (IP) and out-of-phase (OP) experiments are conducted to simulate the temperature, strain, and phase relationship generally [16]; therefore, previous work about TMF of MMCs has been investigated mainly on the influence of phase, the volume fraction of reinforcement, and stress level on the fracture mechanism. Qian et al. [17–19] researched the TMF behavior of SiC_W/6061Al composites with SiC_W volume fraction of 15% and 28% and found that cyclic softening occurred in both composites during IP- and OP-TMF, and the cyclic stress range of high-volume-fraction composites was greater than that of low-volume-fraction composites at an equivalent strain range. In addition, the 15% SiC_W composite revealed a longer life than 28% SiC_W composite in the case of IP-TMF, but the fatigue life curves of the two composites passed across each other in the case of OP-TMF, and the damage mechanism consists of initiation, growth, and coalescence of voids in the matrix around whiskers. Eun [20] reported that the IP-TMF life of Ti-48Al-2V alloy and TiB_2 particles reinforced Ti-48Al-2V composites became longer as the maximum temperature and the stress range decreased, and the TMF mechanism was nucleation and growth of voids on interlamellar plate, twin, and grain boundaries; their interlamellar, translamellar, and intergranular linkage; intergranular separation and disintegration of lamellar structure. The IP- and OP-TMF behavior of SiC_p/Al 2xxx-T4 between 100°C and 300°C composites has been investigated by Karayaka and Sehitoglu [16]. They found that the failure mechanism was creep-fatigue damage in short-life areas and oxidation damage in long-life areas. Sehitoglu [21] found that the TMF life of Al/SiC composites became longer with smaller SiC particle size. It was investigated by Wang et al. that the TMF damage behavior of Al-Si piston alloy was affected by temperature ranges; the cracks mainly initiated from the broken primary silicon in the temperature range of 120~350°C and nucleated from the interface between matrix and primary Si in the temperature range of 120~425°C [22]. However, the effect of particle size and Si contents on the TMF behavior of spray-deposited SiC particles reinforced Al-Si alloy has rarely been investigated.

Thus, the cyclic stress behavior, particulate strengthening mechanism, and thermomechanical fatigue fracture of SiC_p/Al-Si composites in terms of different SiC particle sizes and Si contents were investigated.

2. Experimental Materials and Procedures

The Al-Si alloy and composites reinforced with 15 vol.% SiC particles were prepared by multilayer spray deposition technology; the details of which have been shown in the previous studies [23]. The nominal composition of investigated samples is given in Table 1. The sprayed ingots were extruded at the ratio of 17.3, and T6 heat treatment was performed at 535°C for 2.5 h followed by quenching in room-temperature water and natural aging more than 12 h, finally artificial aging at 160°C for 7 h. All of samples were treated by the abovementioned process.

The machined specimens had a rectangular section of 5 mm × 8 mm and a gauge length of 25 mm, according to ASMT standard E8. TMF tests were examined on a computer-controlled servo hydraulic test machine. As can be seen in Figure 1, the temperature was controlled by triangle wave and detected by thermocouple. Mechanical strain was controlled by cosine waves and measured with 25 mm high-temperature extensometer. The total strain amplitude is 0.3% and R of stress ratio is 0.1. Considering that the disc surface temperature is generally 150-400°C, sometimes up to 450°C [24], specimens were heated using induction heater from minimum temperature of 150°C to a maximum temperature of 400°C. The cycle period (total heating and cooling times) was 100 s for the TMF experiments. After TMF experiments, the fracture morphology was observed by the Quanta 2000 environment scanning electron microscope (SEM).

3. Results

3.1. Microstructure. Some typical phases of Al-7Si alloy and SiC_p/Al-Si composites are identified and marked briefly in the optical micrographs (Figure 2). The Al-7Si alloy is mainly consisted of α-Al matrix and Si particles with white color, which cluster together forming the eutectic Si phase marked in Figure 2(a). SiC particles with an average size of 4.5 μm were distributed evenly in the 4.5μmSiC_p/Al-7Si composite (Figure 2(b)). In Figure 3(c), the SiC particles with grey color and a mean particle size of 20 μm were irregular shaped, and interparticle spacing is smaller than 4.5μmSiC_p/Al-7Si obviously. The morphology of Si phase changed with an increase in Si content; it can be seen a few block-like primary Si phase

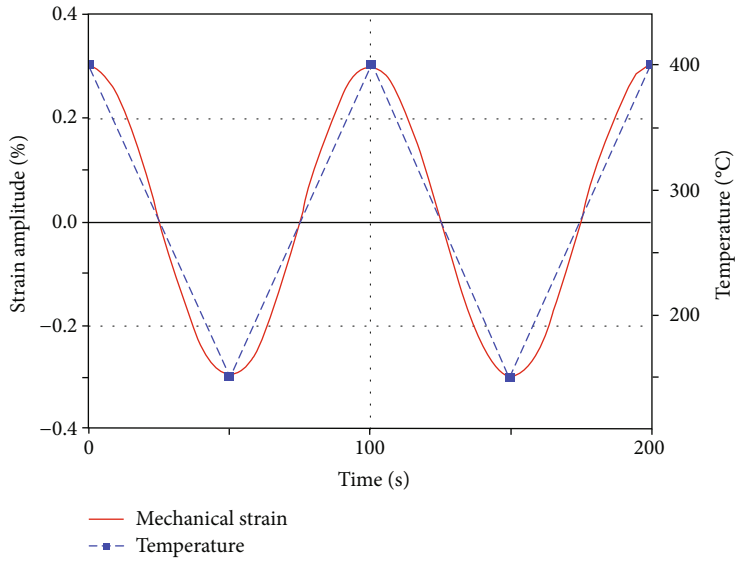

Figure 1: Schematic diagram of IF-TMF.

with an average of 5.85 μm and many round eutectic Si phase with an average of 2.51 μm in the 4.5μmSiC_p/Al-13Si composite (Figure 2(d)). While for 4.5μmSiC_p/Al-20Si composite, the average size of primary Si phase is 7.85 μm and the shape is more random. More details about microstructure have been reported in previous investigations [25, 26].

3.2. Stress-Mechanical Strain Hysteresis Loop. Figure 3 shows the hysteresis loop for the first- and half-life time of SiC_p/Al-7Si composites with different particle sizes during TMF loading. During the heating period of the first cycle, the stress increases with increasing temperature and strain value. When the temperature and strain value first reach the maximum and then both decrease to minimum value, the stress amplitude first reaches the maximum positive value and then decreases to the maximum negative value, correspondingly. In addition, the maximum tensile stress is greater than the maximum compressive stress for the all materials. It can be seen from the Figures 3(a)–3(c) that the stress amplitude of the first cycle life is greater than that of the half-life cycle for all samples, which means that softening occurs once the first cycle begins. Comparison of Figures 2(a)–2(c) shows that the softening degree of Al-7Si alloy is more obvious than other two composites. Especially, the 4.5μmSiC_p/Al-7Si composites have the lowest softening degree.

Typical first- and half-life hysteresis of 4.5μmSiC_p/Al-Si composites with different Si contents for TMF are given in Figure 4. The stress amplitude of the half-life cycle is lower than that of the first cycle life and softening occurs after the first cycle loading for all specimens. It can be also observed that the cyclic softening degree increases with an increase in Si content. The maximum tensile stress is greater than the maximum compressive stress for the same materials during TMF loading process.

3.3. Cyclic Stress Response. Figure 5 shows the cyclic stress response of the studied SiC_p/Al-Si composites at the total mechanical strain amplitude of 0.3%. It can be observed that the cyclic response stress of Al-7Si alloy has the similar trend to those of SiC_p/Al-7Si composites from Figures 5(a) and 5(b), i.e., cyclic softening. While there are a few differences between the details, for Al-7Si alloy, the onset of slight cyclic softening stage occurs from 1 to 10 cycles, and then the softening degree becomes more significant, and finally rapid softening occurred from about 300 cycles to rupture time. For 4.5μmSiC_p/Al-7Si composite, rapid cyclic softening occurs during the first 20 cycles, nearly followed by saturation around 700 cycles and rapid softening till failure. The 20μmSiC_p/Al-7Si composites show rapid cyclic softening during the first 30 cycles, followed by slight softening till about 800 cycles and then failure. In addition, the stress ranges are the largest in the first cycle and then decrease rapidly in the following cycles for all samples. It can be found that the stress amplitude of Al-7Si alloy is obviously lower than that of SiC particle-reinforced Al-7Si composites, of which the stress amplitude of 20μmSiC_p/Al-7Si composite is the highest. Thereafter, it is worth noting that an increase in SiC particle size leads to an increase in the TMF life. The 4.5μmSiC_p/Al-Si composites with different Si content also exhibit softening tendency from initial cycles to final rupture, and an increase in Si content results in a more pronounced cycle softening (Figure 5(b)). In terms of stress amplitude, a similar trend also appears. The higher the Si content, the greater the stress amplitude. However, there is no significant difference in the TMF life of these composites; the TMF life of 4.5μmSiC_p/Al-7Si composite is slightly longer than the other two composites, while the TMF life of 4.5μmSiC_p/Al-13Si composites and 4.5μmSiC_p/Al-20Si composites is similar.

3.4. Fractographical Observation. The TMF fractography of Al-7Si alloy and SiC_p/Al-Si composites is shown in Figure 6. The rough fracture surface consists of many micropores with 3-5 μm in size uniformly distributed in the region of stable fatigue crack propagation (Figure 6(a)). Figure 6(b) is the magnified view of the region of fatigue crack

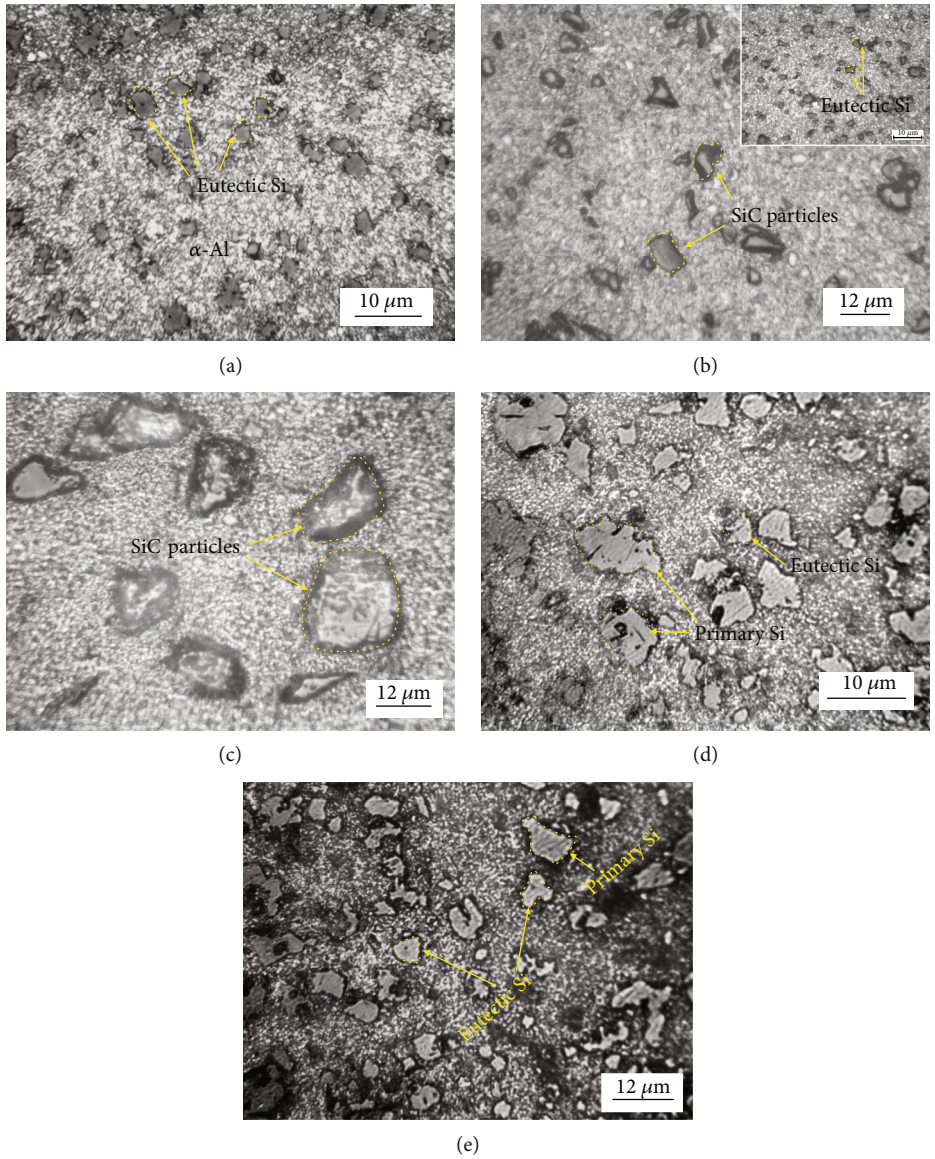

Figure 2: Microstructures of (a) Al-7Si alloy; (b) 4.5μmSiC_p/Al-7Si (eutectic); (c) 20μmSiC_p/Al-7Si; (d) 4.5μmSiC_p/Al-13Si (eutectic); (e) 4.5μmSiC_p/Al-20Si (hypereutectic).

propagation, and there are many small eutectic Si particles scattering around the micropores, which is probably associated with debonding during TMF loading. Crack tip factor increases as the cycles increases, which results in the sharp rising amount of micropores and dimples. Fatigue striation and micropores distributed alternatively on the rough fracture surface of 4.5μmSiC_p/Al-7Si composite can be presented in Figure 6(c), and the direction of fatigue crack propagation is perpendicular to fatigue striation. Plenty of complete SiC particles and several Si particles can be observed at transient fracture zone (Figure 6(d)), which indicates that SiC particles debond from Al-Si matrix and form aggregation accelerating fatigue crack initiation and propagation during TMF loading. Figure 6(e) shows rougher fracture surface of 20μmSiC_p/Al-7Si composites in the region of crack propagation than that of Al-7Si alloy and 4.5μmSiC_p/Al-7Si composite, and the propagation paths are more tortuous. There are some broken primary SiC particles distributing on the fracture plane, where the decohesion of SiC particles and Si particles also occurs peripherally. Besides, many voids form around the particles, and cavities and pits accumulate together with the increase in TMF cycles. The contiguous holes interlink with each other due to the tearing of different phases in the monolithic alloy, thus forming many microcracks (Figure 6(f)).

Similar to 4.5μmSiC_p/Al-7Si composite, typical fatigue striation should have been observed in the region of crack propagation for the 4.5μmSiC_p/Al-13Si composite; however, there is no such characterization probably because some free SiC particles and Si phases concealed the fatigue striation, but plenty of homogeneous cavities and dimples also can be seen in the fracture surface. These SiC particles agglomerate together more tightly to form a large cluster, like a big

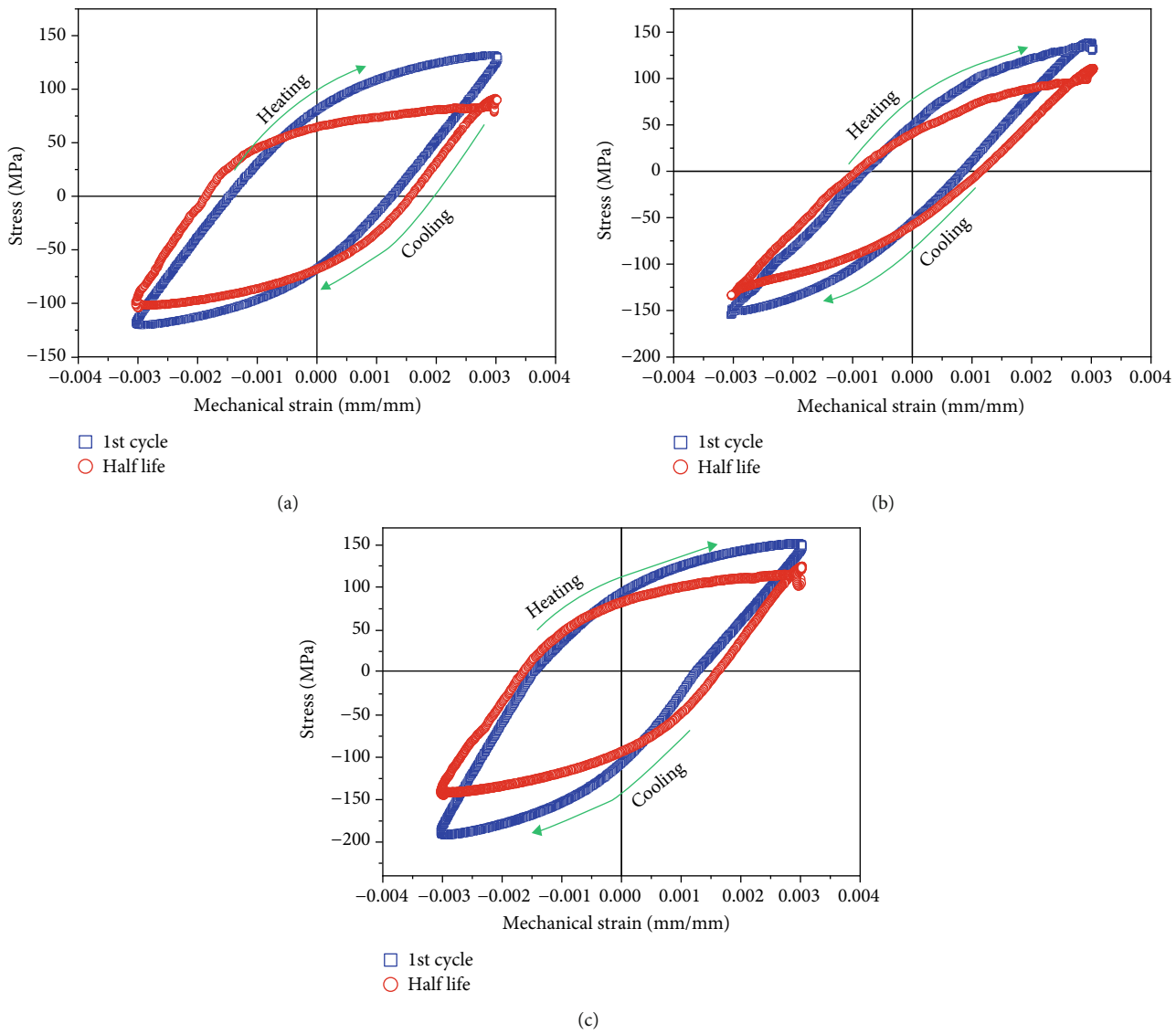

FIGURE 3: The stress-mechanical strain hysteresis loop of (a) Al-7Si alloy; (b) 4.5μmSiC$_p$/Al-7Si composite; (c) 20μmSiC$_p$/Al-7Si composite ($\Delta\varepsilon_m = 0.3\%$).

particle, which results in the crack initiation more easily (Figure 6(g)). In addition, the fracture of some free primary Si possibly takes place at crack growth stage (Figure 6(h)). The striations and cavities appear alternatively in the TMF fractographs of 4.5μmSiC$_p$/Al-20Si composites (Figure 6(i)), and the reason for the formation of cavities may be related to SiC particles and Si particles debonding from Al-Si matrix. The size of primary Si particles increases as Si content increases, and cracks nucleate primary Si particles with larger size, which results in many microcracks in Figure 6(j).

4. Discussion

4.1. The Effect of Thermal Expansion Coefficient on Fatigue Life. Karayaka and Sehitoglu [16] investigated the thermomechanical fatigue of metal matrix composite and found that temperature and mechanical strain always changed momentarily in the TMF process. Lloyd [27] also pointed out that the total strain was the sum of thermal and mechanical strain components:

$$\varepsilon_{net} = \varepsilon_{th} + \varepsilon_{mech} = \alpha(T - T_0) + \varepsilon_{mech}, \quad (1)$$

where ε_{net} is the total strain, ε_{th} is the thermal strain, ε_{mech} is the mechanical strain, T_0 is the initial temperature at the beginning of experiment, T is the real-time temperature of experiment, and α is the thermal expansion coefficient of composites.

SiC$_p$/Al-Si composites are composed of the Al matrix, Si phases, and SiC particles. The difference in Si content and SiC particle size will lead to a great difference in thermal expansion coefficient of materials, which will directly affect the dislocation and residual internal stress of materials. Elomari et al. [28] indicated that the addition of SiC reinforced particles could effectively reduce the thermal expansion

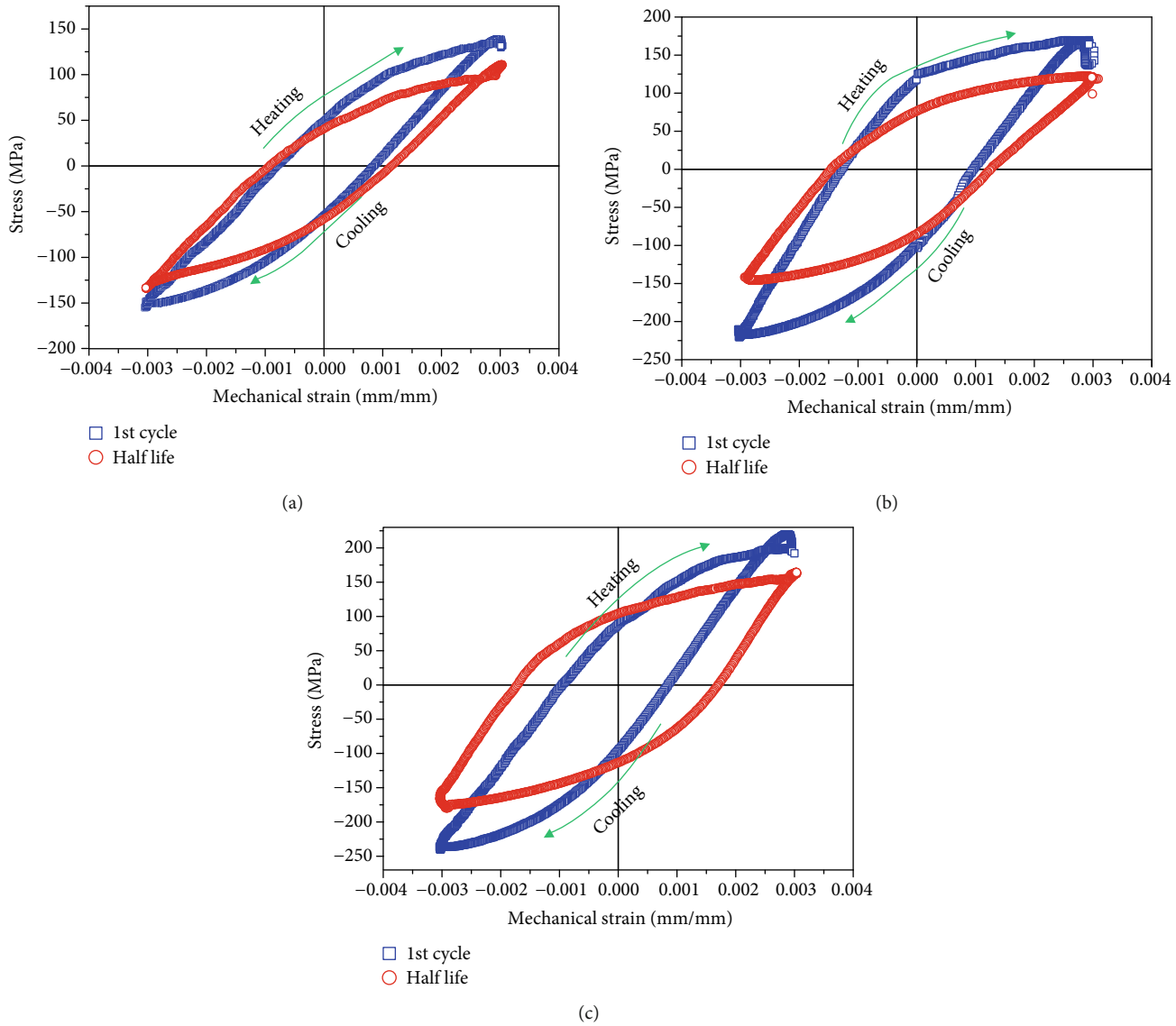

Figure 4: The stress-mechanical strain hysteresis loop of (a) 4.5μmSiC$_p$/Al-Si composite; (b) 4.5μmSiC$_p$/Al-13Si composite; (c) 4.5μmSiC$_p$/Al-20Si composite ($\Delta\varepsilon_m = 0.3\%$).

coefficient of the material. When the volume fraction of reinforced particles was constant, the thermal expansion coefficient of composites decreased with the decrease of SiC particle size. Thus, it can be concluded that the thermal expansion coefficient of Al-7Si alloy in this paper is the highest, followed by composite with 20 μm SiC particles and composite reinforced with 4.5 μm SiC particles. When the cyclic loading temperature is applied between 150 and 400°C, the Al-7Si alloy exhibited the most obvious thermoplastic deformation, which is attributed to the highest thermal strain and residual thermal stress, leading to the lowest fatigue life.

4.2. The Effect of SiC Particle Size. The stress amplitude and TMF life of SiC$_p$/Al-7Si composite are both greater than that of Al-7Si alloy, which is closely related to the strengthening mechanism of reinforced particles. Generally, there are two kinds of strengthening mechanisms, direct strengthening and indirect strengthening. The load transmission between matrix and reinforced particles is taken into account for direct strengthening, and the effect of reinforcement on microstructure and deformation mode of matrix is concerned about indirect strengthening [29]. From the perspective of direct strengthening, elastic modulus of matrix is lower than that of SiC particles; thus, SiC particles can undertake the loading partly from matrix, which improves the strength of materials. According to the shear lag model proposed by Nardone and Prewo [30],

$$\sigma_{cy} = \sigma_{my}\left(\frac{V_p(S+4)}{4} + V_m\right), \tag{2}$$

where σ_{cy} is the yield strength of composites, σ_{my} is the yield strength of alloys, S is the length-to-diameter aspect ratio of reinforced particles, and V_p and V_m are the volume fraction of reinforced particles and matrix, respectively.

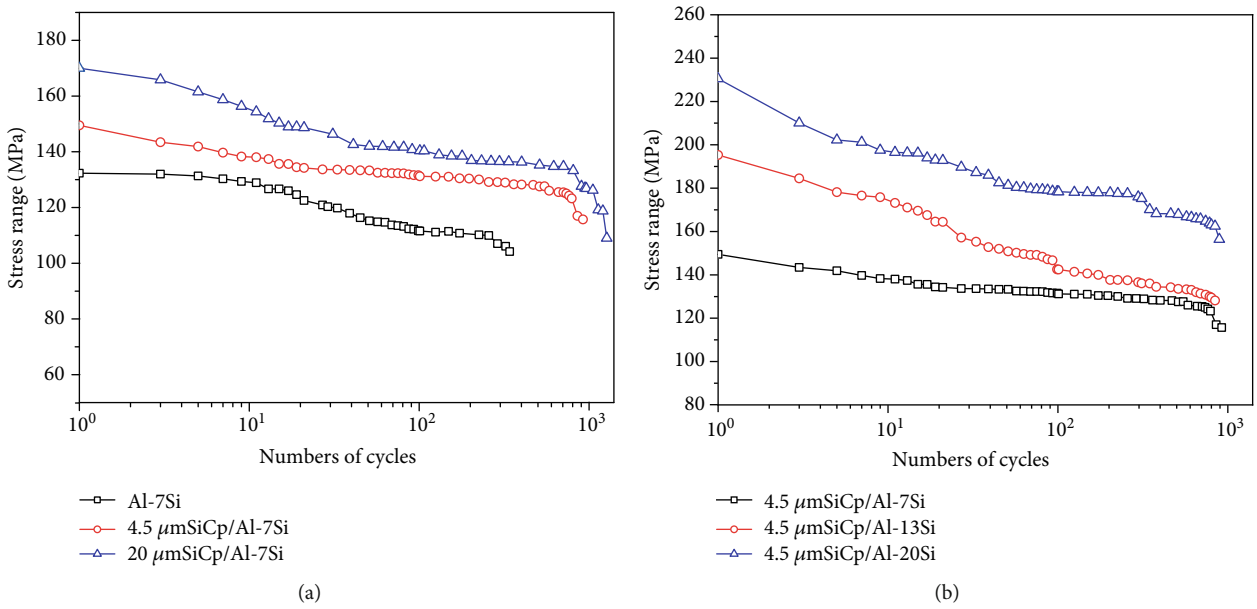

FIGURE 5: Cyclic stress response curves of SiC_p/Al-Si composite ($\Delta\varepsilon_m = 0.3\%$).

In accordance with the microstructure of SiC_p/Al-7Si composites, the aspect ratio S can be measured to be 1.38 and 1.94 for 4.5 μm SiC particle and 20 μm SiC particles, respectively. It can be calculated from formula (2) that composite with 20 μm SiC reinforcement exhibits the highest yield strength, which is consistent with the mechanical properties measured experimentally in literature [23], leading to a higher cyclic stress response.

In this study, the indirect strengthening mainly caused by the geometric dislocation resulted from the mismatch of the thermal expansion coefficient between the refractory-phase reinforced particles SiC and the deformable-phase Al-7Si alloy. Especially, the thermal expansion coefficient induced by smaller particles results in higher geometrically dislocation density, discussed in Ref. [21]. Consequently, the geometrically dislocation density of 4.5μmSiC_p/Al-7Si composite is greater than that of 20μmSiC_p/Al-7Si composite. Based on the constitutive relationship between shear flow stress and dislocation proposed by Fleck et al. [31],

$$\tau = \kappa G b \sqrt{\rho} \tag{3}$$

where G is the elastic modulus of Al-7Si alloy, GPa; κ is the scalar coefficient; b is the Burgers vector. Thus, the increase in dislocation density results in an increase in flow stress, namely, the yield strength of 4.5μmSiC_p/Al-7Si composite is greater than that of 20μmSiC_p/Al-7Si composite; in ordinary, the TMF behaviors have the same rule as yield strength. Similar results are also reported in Ref. [21]. However, the observations in cyclic stress response are different from the above accepted point, which could be predominantly correlated to the lower yield strength resulted from the formation of fine particle clusters [23]. Load transfers from the matrix to the SiC particles in the TMF process, but when the aggregated SiC particles form loose microstructure, crack initiation and propagation occur more easily, which accelerates the failure of the material. While SiC particles are distributed uniformly in the 20μmSiC_p/Al-7Si composite, cracks initiate the defects of particles. Reference [24] indicates that the SiC particles with small size result in void nucleation, increasing the low-cycle fatigue life at the high strain amplitude (>0.3%). In summary, the direct strengthening mechanism is dominant in Al-7Si alloy and SiC_p/Al-7Si composites.

4.3. The Effect of Si Content. Generally, the Si species, including primary Si phase and eutectic Si phase, differ from Si contents in composites, which results in different TMF properties. The microstructure of 4.5μmSiC_p/Al-Si composites shows that the volume fraction and average size of Si phase increase with an increase in Si content. The SEM images of the fracture surface on the TMF samples indicate two distinctly crack growth mechanisms of primary Si particle and eutectic Si, which are summarized in Figure 7. It can be described that the TMF cracks will propagate through the primary Si particles and along the interface between eutectic Si and α-Al matrix, which is related to the crack-tip driving forces [32]. Besides, continuous thermal cycle will result in expansion of Si particles and local microplasticity around the α-Al/Si interface accelerating the deformation of composites, the concept has also been reported in Ref. [22]. Therefore, in this study, the fracture modes of 4.5μmSiC_p/Al-7Si composite are debonding and aggregation of SiC particles, along with the detachment of eutectic Si phase, while for 4.5μmSiC_p/Al-13Si composite, the detachment of eutectic Si phase is the main fracture mode; meanwhile, the broken primary Si phases are very rare. The fracture tendency of primary Si increases with increasing Si content; thus, plenty broken primary Si phases can be seen for 4.5μmSiC_p/Al-20Si composite. In addition, the loading distribution between particles and matrix is largely decided by the Si interparticle distance, and the interparticle

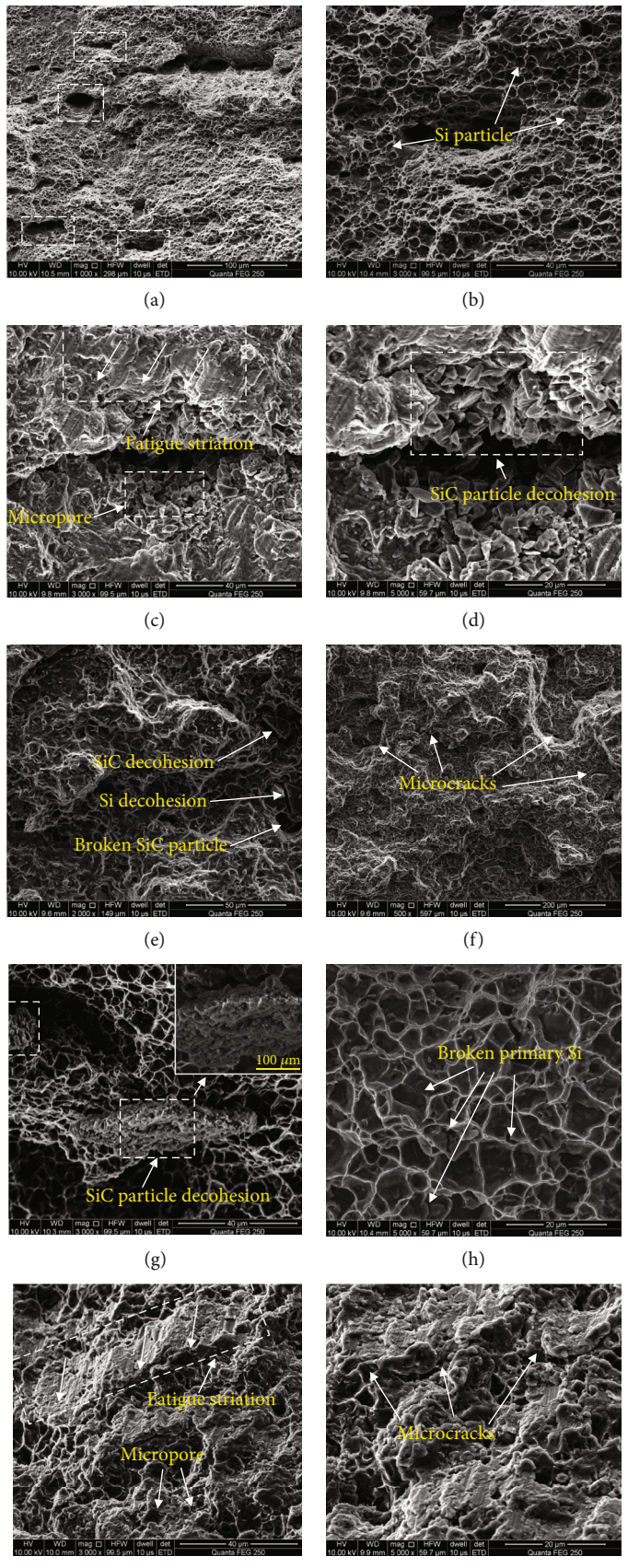

Figure 6: SEM micrograph of samples of TMF fracture surface (a, b) Al-7Si; (c, d) 4.5μmSiC_p/Al-7Si; (e, f) 20μmSiC_p/Al-7Si; (g, h) 4.5μmSiC_p/Al-13Si; (i, j) 4.5μmSiC_p/Al-20Si.

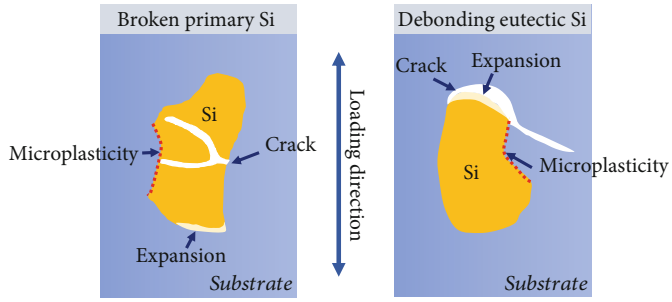

Figure 7: Schematic of the TMF crack growth mechanism.

distance of 4.5μmSiC$_p$/Al-20Si composite is the smallest. Once the plastic deformation occurs in the local matrix, Si phase can impede the dislocation sliding movement due to more difficult deformation than α-Al matrix, which can slow down the overall plastic deformation of composite. Therefore, 4.5μmSiC$_p$/Al-20Si composite possesses the best performance to resist the plastic deformation. Moreover, the stress amplitude of composite, which meets the movable dislocation amount bypassing the obstacles, increases with increasing Si content; therefore, the stress amplitude of 4.5μmSiC$_p$/Al-20Si composites is the highest.

When the composite is cooled from high temperature or processing, the α-Al matrix near the Si phase and SiC particles is easily deformed; thus, dislocations are generated, moved, and stored. The main reason of dislocation generation is differential thermal contraction at the Al-Si-SiC$_p$ interface due to the CTE mismatch among α-Al matrix, Si phase, and SiC particles [33, 34]. If the size and volume fraction of SiC particles is constant, the effect of Si content on the dislocation should be considered carefully. Figure 8 is the schematic of geometrically necessary dislocation model. Assuming that (1) the Al-Si-SiC interface is well-bonded and (2) Si particles and SiC particles are simplified as sphere, the strain gradient is produced in the transition area from the Si-phase interface to the region far away the interface in the matrix; thus, the geometrically necessary dislocation decreases with the increasing interparticle spacing, namely, the $\lambda/2$ in Figure 8. It can be examined that the interparticle distance (λ) of Si phase increases with Si content in Figure 2. In addition, the presence of strain gradient results in geometrically necessary dislocation to adapt to lattice distortion for composites, and the relationship can be expressed as formula (4) proposed by Arsenlis and Parks [35]:

$$\rho^{G} = \frac{N\eta}{b}, \tag{4}$$

where ρ^{G} is the geometrically necessary dislocation, N is the Nye factor, and usually $N = 2$ for polycrystalline materials, η is the strain gradient, and b is the Burgers vector. Therefore, the geometrically necessary dislocation increases as the strain gradient increases, the same to Si contents. Therefore, the dislocation density of 4.5μmSiC$_p$/Al-20Si composite is the greatest, which is the dominant reason of high-degree softening.

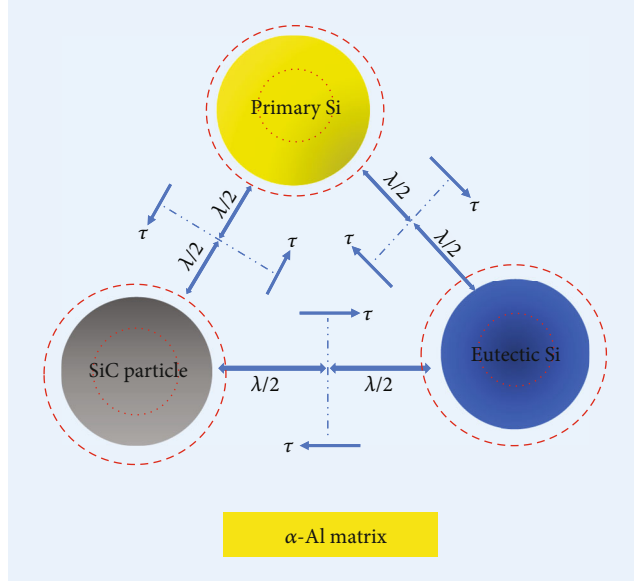

Figure 8: Schematic of geometrically necessary dislocation model.

5. Conclusion

The thermomechanical fatigue behaviors of spray-deposited SiC$_p$/Al-Si composites were investigated in terms of the size of SiC particles and the Si content in the temperature range of 150-400°C. The main findings are listed below:

(1) Hysteresis loop reveals that the stress amplitude of the first cycle life is greater than that of the half-life cycle for all samples, which means that softening occurs since the first cycle begins. And the maximum compressive stress is generally lower than the maximum tensile stress for the same materials during TMF loading process

(2) There exists a continuous cyclic softening in Al-7Si alloy and SiC$_p$/Al-Si composite. Both the increase in SiC particle size and Si content can aggravate the softening degree obviously, which is correlated with the dislocation generation in differential thermal contraction at the Al matrix/Si phase and Al matrix/SiC particles. Besides, the stress amplitude of SiC$_p$/Al-7Si composites increases with increasing SiC particle size or Si content, which is attributed to the abilities to meet the movable dislocation amount bypassing the obstacles

(3) The TMF life is remarkably enhanced by an increase in SiC particle size, which is associated with "load sharing" of the direct strengthening mechanism. Nevertheless, little or no influence on the TMF life is found through increasing Si content

(4) Compared to Al-7Si alloy and 4.5μmSiC_p/Al-7Si composite, 20μmSiC_p/Al-7Si composite presents a rougher fracture surface in the region of crack propagation. As Si content increases, the fracture tendency of primary Si increases, resulting in an increase in microcrack nucleation. The failure mechanism of SiC_p/Al-7Si composites reveals that the agglomeration of small-particulate SiC and the breakage of large-particulate SiC are the main crack initiation sites. The broken primary Si and the exfoliated eutectic Si accelerate the crack propagation

Data Availability

All data used to sustain the findings of this study are included in the article.

Conflicts of Interest

The authors declare that they have no conflicts of interest.

Acknowledgments

The authors received financial support from the National Natural Science Foundation of China (No. 51675058), the Key Scientific Research Project of the Education Department of Hunan Province (No. 16A002), the Science and Technology Innovation Project of Hunan Province (No. 2018RS3073) and the Natural Science Foundation of Hunan Province (No. 2018JJ3531), and the Double First-Class Scientific Research International Cooperation Project of Changsha University of Science and Technology (2019IC15).

References

[1] M. Kenisarin and K. Mahkamov, "Solar energy storage using phase change materials," *Renewable and Sustainable Energy Reviews*, vol. 11, no. 9, pp. 1913–1965, 2007.

[2] A. Adamowicz and P. Grzes, "Influence of convective cooling on a disc brake temperature distribution during repetitive braking," *Applied Thermal Engineering*, vol. 31, no. 14-15, pp. 2177–2185, 2011.

[3] C. Li, L. Qin, M. Li, H. Xiao, Q. Wang, and J. Chen, "Influence of deformation strain rate on the mechanical response in a metastable β titanium alloy with various microstructures," *Journal of Alloy Compounds*, vol. 815, article 152426, 2020.

[4] C. Li, H. Li, and S. van der Zwaag, "Unravelling the abrasion resistance of two novel meta-stable titanium alloys on the basis of multi-pass-dual-indenter tests," *Wear*, vol. 440-441, p. 203094, 2019.

[5] W. Li, Y. Ning, J. Chen, Y. Sun, Y. Hu, and J. He, "Investigation on microstructure and fatigue characteristics of spray-formed SiC_p/Al–20Si composite," *Transactions of the Indian Institute of Metals*, vol. 68, no. 5, pp. 769–775, 2015.

[6] W. Li, Y. Ning, J. Chen, Y. P. Sun, and C. Li, "Effect of Si content on microstructure and mechanical properties of the spray-formed SiC_p/Al–Si composites," *Powder Metallurgy and Metal Ceramics*, vol. 54, no. 5-6, pp. 298–303, 2015.

[7] W. Li, J. Chen, J. J. He et al., "Effect of the SiC particle orientation anisotropy on the tensile properties of a spray-formed SiCp/Al-Si composite," *Strength of Materials*, vol. 46, no. 2, pp. 221–228, 2014.

[8] W. Li, Z. H. Chen, D. Chen, and J. Teng, "Growth behavior of fatigue crack in spray-formed SiC_p/Al-7Si composite," *Acta Metallurgica Sinica*, vol. 47, no. 1, pp. 102–108, 2011.

[9] S. Y. Wang, Q. Tang, D. J. Li et al., "The hot workability of SiC_p/2024 Al composite by stir casting," *Materials and Manufacturing Processes*, vol. 30, no. 5, pp. 624–630, 2015.

[10] M. Günay and U. Şeker, "Evaluation of surface integrity during machining with different tool grades of Sic_p/Al-Si composites produced by powder metallurgy," *Materials Science Forum*, vol. 672, pp. 319–322, 2011.

[11] Y. P. Sun, J. Han, Y. Tu, Z. Bai, and Y. Q. He, "Microstructure and mechanical properties of a spray deposited SiC_p/Al composite processed by hot extrusion and equal channel angular pressing," *Materials Research Innovations*, vol. 18, Supplement 4, pp. S4-220–S4-223, 2014.

[12] E. J. Lavernia and N. J. Grant, "Spray deposition of metals: a review," *Materials Science and Engineering*, vol. 98, pp. 381–394, 1988.

[13] R. Yang, X. J. Wang, X. P. Wu, M. H. Chen, N. Liu, and Q. W. Li, "Progress in stir-casting process for fabricating SiC_p/Al composites," *Materials Review*, vol. 27, no. 9, pp. 131–136, 2013.

[14] W. B. Hu, C. C. Jia, B. F. Hu, and G. F. Tian, "The previous particle boundaries (PPB) of FGH96 superalloy and its effects on impact property," *Powder Metallurgy Technology*, vol. 30, no. 5, pp. 327–333, 2012.

[15] J. L. Estrada, "Microstructure characterization of Al-Si and MMCs preforms processed by spray atomization and deposition," *Journal of Materials Science*, vol. 33, no. 16, pp. 4029–4033, 1998.

[16] M. Karayaka and H. Sehitoglu, "Thermo-mechanical fatigue of metal matrix composites," *Low Cycle Fatigue and Elasto-Plastic Behaviour of Materials—3*, pp. 13–18, Springer, Netherlands, 1992.

[17] L. H. Qian, Z. G. Wang, H. Toda, and T. Kobayashi, "Thermo-mechanical fatigue of SiC whisker reinforced 6061Al composites: I. Stress and strain during cycling," *Acta Metallurgica Sinica*, vol. 37, no. 11, pp. 1198–1202, 2001.

[18] L. H. Qian, Z. G. Wang, H. Toda, and T. Kobayashi, "Thermo-mechanical fatigue of SiC whisker reinforced 6061al composites: II. Fatigue life and damage," *Acta Metallurgica Sinica*, vol. 37, no. 11, pp. 1206-1207, 2001.

[19] L. H. Qian, Z. G. Wang, H. Toda, and T. Kobayashi, "Effect of reinforcement volume fraction on the thermo-mechanical fatigue behavior of SiC_w/6061Al composites," *Materials Science and Engineering: A*, vol. 357, no. 1-2, pp. 240–247, 2003.

[20] L. U. Eun, "Thermal-mechanical fatigue of Ti-48Al-2V alloy and its composite," *Metallurgical and Materials Transactions A*, vol. 25, no. 10, article 2207, 1994.

[21] H. Sehitoglu, "The effect of particle size on thermo-mechanical fatigue of Al/SiC metal matrix composites," *Fatigue under*

Thermal and Mechanical Loading: Mechanisms, Mechanics and Modelling, pp. 371–380, Springer, Netherlands, 1996.

[22] M. Wang, J. C. Pang, M. X. Zhang, H. Q. Liu, S. X. Li, and Z. F. Zhang, "Thermo-mechanical fatigue behavior and life prediction of the Al-Si piston alloy," *Materials Science and Engineering: A*, vol. 715, pp. 62–72, 2018.

[23] W. Li, Z. H. Chen, D. Chen, J. Teng, and L. Changhao, "Understanding the influence of particle size on strain versus fatigue life, and fracture behavior of aluminum alloy composites produced by spray deposition," *Journal of Materials Science*, vol. 46, no. 5, pp. 1153–1160, 2011.

[24] L. A. Boatner, J. S. Neal, J. A. Kolopus, J. O. Ramey, and H. Akkurt, "The characterization of scintillator performance at temperatures up to 400 degrees centigrade," *Nuclear Instruments and Methods in Physics Research Section A: Accelerators, Spectrometers, Detectors and Associated Equipment*, vol. 709, pp. 95–107, 2013.

[25] W. Li, C. Jian, Y. Hu, L. Cong, Y. P. Sun, and J. M. Yang, "Cyclic fatigue fracture behavior of spray-deposited SiC_p/Al-Si composite," *Journal of Materials Engineering and Performance*, vol. 23, no. 8, pp. 2871–2876, 2014.

[26] W. Li, Z. H. Chen, D. Chen, J. Teng, and C. Fan, "Low-cycle fatigue behavior of SiC_p/Al-Si composites produced by spray deposition," *Materials Science and Engineering: A*, vol. 527, no. 29-30, pp. 7631–7637, 2010.

[27] D. J. Lloyd, "Particle reinforced aluminium and magnesium matrix composites," *International Materials Reviews*, vol. 39, no. 1, pp. 1–23, 1994.

[28] S. Elomari, M. D. Skibo, A. Sundarrajan, and H. Richards, "Thermal expansion behavior of particulate metal-matrix composites," *Composites Science and Technology*, vol. 58, no. 3-4, pp. 369–376, 1998.

[29] J. E. Allison and J. W. Jones, "Chapter 15 – fatigue behavior of discontinuously reinforced metal-matrix composites," *Fundamentals of Metal-Matrix Composites*, vol. 14, no. 3, pp. 269–294, 1993.

[30] V. C. Nardone and K. Prewo, "On the strength of discontinuous silicon carbide reinforced aluminum composites," *Scripta Metallurgica*, vol. 20, no. 1, pp. 43–48, 1986.

[31] N. A. Fleck, G. M. Muller, M. F. Ashby, and J. W. Hutchinson, "Strain gradient plasticity: theory and experiment," *Acta Metallurgica et Materialia*, vol. 42, no. 2, pp. 475–487, 1994.

[32] K. Gall, N. Yang, M. Horstemeyer, D. L. McDowell, and J. Fan, "The debonding and fracture of Si particles during the fatigue of a cast Al-Si alloy," *Metallurgical and Materials Transactions A*, vol. 30, no. 12, pp. 3079–3088, 1999.

[33] M. Kouzeli and A. Mortensen, "Size dependent strengthening in particle reinforced aluminium," *Acta Materialia*, vol. 50, no. 1, pp. 39–51, 2002.

[34] R. J. Arsenault and N. Shi, "Dislocation generation due to differences between the coefficients of thermal expansion," *Materials Science and Engineering*, vol. 81, pp. 175–187, 1986.

[35] A. Arsenlis and D. M. Parks, "Crystallographic aspects of geometrically-necessary and statistically-stored dislocation density," *Acta Materialia*, vol. 47, no. 5, pp. 1597–1611, 1999.